Asia-Pacific Journal of Atmospheric Sciences
https://doi.org/10.1007/s13143-022-00308-y

Online ISSN 1976-7951
Print ISSN 1976-7633

ORIGINAL ARTICLE

Exceptionally persistent Eurasian cold events and their stratospheric link

Kathrin Finke[1,2] · **Abdel Hannachi**[1,2] · **Toshihiko Hirooka**[3]

Received: 09 September 2022 / Revised: 20 November 2022 / Accepted: 25 November 2022

Abstract

Persistent boreal winter cold spells (PCEs) can heavily strain the economy and significantly impact everyday life. While sudden stratospheric warmings are considered a precursor for Eurasian (EUR) cold events, these temperature extremes may occur during the full range of stratospheric variability. We investigate PCEs relative to the prevailing stratospheric polar vortex regime before their onset, with a particular focus on extremely weak (SSW) and strong (SPV) stratospheric winds by performing (lagged) composite analysis based on ERA5 reanalysis. On average, SPV PCEs that are concentrated over central EUR, are colder, shorter and set in more abruptly compared to SSW PCEs. A quasi-stationary, mid-tropospheric anticyclone over the Arctic Ocean that blocks warm air advection toward EUR is connected to the canonical downward progression of the negative North Atlantic Oscillation for SSW PCEs. In contrast, during SPV PCEs, the anticyclone is part of a Rossby wave having an origin co-located with negative wave activity flux anomalies over and being influenced by stratospheric wave reflection toward the North Atlantic. Its slow east-ward propagation is likely related to Arctic surface warming and unusually weak zonal winds over EUR.

Keywords Cold spells · Sudden stratospheric warming · Eurasia · Wave activity fluxes · Blocking · Extreme events

1 Introduction

Extremely cold temperatures in winter-time Eurasia are known to heavily strain the infrastructure, society and economy, and harshly impact everyday life. Increasing preparedness as early as possible before their onset is thus of major scientific and societal interest, driving research on their timely prediction.

Locally, Eurasian winter-time, cold surface temperatures have been, for example, associated with Arctic sea ice loss, yielding an amplification of the Siberian High (e.g. Panagiotopoulos et al. 2005; Honda et al. 2009; Wu et al. 2011) and driving Ural blocking (e.g. Yao et al. 2017), thereby promoting cold air advection toward Eurasia (e.g. Mori et al. 2014).

From a remote perspective, Eurasian weather has been shown to be strongly influenced by the circulation over the North Atlantic (e.g. Barnett et al. 1984) whose extended-range predictability can be inferred from the dynamic state of the stratosphere (e.g. Domeisen et al. 2020). In winter, increased radiative cooling over the pole facilitates strong temperature contrasts between the mid-latitude and polar stratosphere, resulting in strong, quasi-zonal, circumpolar westerlies (Waugh and Polvani 2010; Waugh et al. 2017). Vertically propagating planetary waves from the troposphere may deposit easterly momentum onto the stratospheric polar vortex (McIntyre and Palmer 1983) via wave breaking (Charney and Drazin 1961), thereby disturbing the geostrophically balanced flow and fostering an abrupt increase of polar cap temperatures (e.g. Matsuno 1971; O'Neill et al. 2015). Positive polar cap temperature as well as geopotential height anomalies, corresponding to the negative phase of the Northern Annular Mode, may migrate downward into the troposphere (e.g. Baldwin and Dunkerton 1999, 2001; Thompson et al. 2002; Hitchcock

Communicated by: Christian Franzke

✉ Kathrin Finke
kathrin.finke@misu.su.se

[1] Department of Meteorology, MISU, Stockholm University, Stockholm, Sweden

[2] Bolin Centre for Climate Research, Stockholm University, Stockholm, Sweden

[3] Department of Earth and Planetary Sciences, Kyushu University, Fukuoka, Japan

and Simpson 2014; Kodera et al. 2016) through wave-mean-flow interaction, manifesting at the surface as the negative phase of the Arctic Oscillation and the North Atlantic Oscillation (NAO) (e.g. Baldwin and Dunkerton 2001; Hitchcock and Simpson 2014). Cold Northern European and Eurasian surface temperature anomalies may develop in response (Thompson and Wallace 2001; Kretschmer et al. 2018a, 2018b; King et al. 2019; Finke and Hannachi 2022), that have an increased predictability through this stratosphere-troposphere coupling (Statnaia et al. 2022). Further, a reduction in meridional temperature, and thus, geopotential height gradient due to an unusually warm Arctic may decrease large-amplitude Rossby wave progression over the North Atlantic, potentially increasing the persistence of e.g. downstream cold spells (Francis and Vavrus 2012). Chen et al. (2021) found Ural blocking to be more persistent when Barents-Kara sea warming is weak, while a strong warming yields a weakened stratospheric polar vortex with a negative NAO response and subsequent downstream progression of Ural blocking.

A non-zonally symmetric configuration (Kodera et al. 2008, 2013, 2016; Kretschmer et al. 2018b) or an unusually strong polar vortex in the high-latitude stratosphere (e.g. Perlwitz and Graf 2001; Perlwitz and Harnik 2003, 2004), resulting from undisturbed radiative cooling, instead, may constrain the upward wave propagation by allocating a layer that reflects planetary waves back down to the troposphere where they may influence the structure of planetary waves (Perlwitz and Harnik 2004). The consequent channeling of planetary waves in the troposphere fosters the development of the positive phase of the Northern Annular Mode and NAO (e.g. Baldwin and Dunkerton 2001; Scaife et al. 2005) corresponding to warm surface temperature anomalies in northern Europe and eastern Asia (Thompson et al. 2002).

Stratospheric polar vortex variability in the sense of changes in mid-stratospheric zonal mean zonal wind, can thus yield surface temperature changes in Eurasia, i.e. cold (warm) temperature anomalies have been linked to a weak (strong) stratospheric polar vortex. However, Eurasian cold spells may also occur during episodes with unusually strong stratospheric vortex conditions. We explore common and distinctive statistical and dynamical characteristics of persistent Eurasian cold spells after strong and weak polar vortex events. The top-to-bottom approach has been used extensively to study the stratosphere-troposphere connection. Complementing, our study is based on a bottom-up approach, i.e. analysis based on the time evolution of the tropospheric event, thus enlarging the comprehensive understanding of mechanisms inducing Eurasian cold spells, ultimately aiming for an improvement of their extended-range prediction.

2 Data and Methods

2.1 Data

In the present study, daily averages of 6-hourly ERA5 reanalysis data (Hersbach et al. 2020) are considered. The data consist of sea level pressure (SLP), geopotential, 3D wind and 2m air temperature (T2m), for the 40-year time period from 1979 to 2019 for the November to March (NDJFM) season on a $1° \times 1°$ regular latitude-longitude grid and 37 pressure levels from 1000hPa to 1hPa. The 29th February is excluded from the analysis.

2.2 Methodology

2.2.1 Study Region

The objective of the study is to identify and classify cold extremes and investigate their potential linkage to stratospheric variability. An empirical orthogonal function (EOF) analysis has been applied to the 5-day running mean T2m anomalies with respect to their climatology, i.e. 40-year daily mean, spatially bounded between the 20°N and 90°N latitude, to identify a geographical region of interest in Eurasia. Composites of T2m anomalies for the first 4 modes of variability, explaining 11.65%, 11.05%, 7.67% and 6.37%, respectively, for the corresponding standardized principle components (PC) with values higher than 1, are shown in Fig. 1. The black box, located over a vast region of Eurasia (EUR) [50°N – 65°N; 15°E – 130°E], identifies the study region that was chosen based on the main regions of variability corresponding to EOF1, EOF3 and EOF4. Accordingly, T2m anomaly composites based on days with PC1 $>$ 1 (a), PC3 $>$ 1 (c) and PC4 $>$ 1 (d) reflect cold temperatures over parts of Eurasia. The region over the eastern US, emerging in PC2 $>$ 1 (b), PC3 $>$ 1 and PC4 $>$ 1, is left for future research.

2.2.2 Construction of Indices and Event Classification

The daily, 5-day running mean T2m is latitude-weighted by multiplication of each grid point value by the square-root of the cosine of latitude before averaging over EUR to construct an index that is shown in Fig. 1e. We find a distribution with significant negative skewness (-0.23), indicating a longer tail on the cold temperature side and reflecting the intermittent occurrence of extreme cold events. A persistent cold event (PCE) is defined if the T2m index is below one standard deviation (-2.53K; dark blue values in Fig. 1e) for at least 6 consecutive days of which the first day of threshold exceedence is taken as the

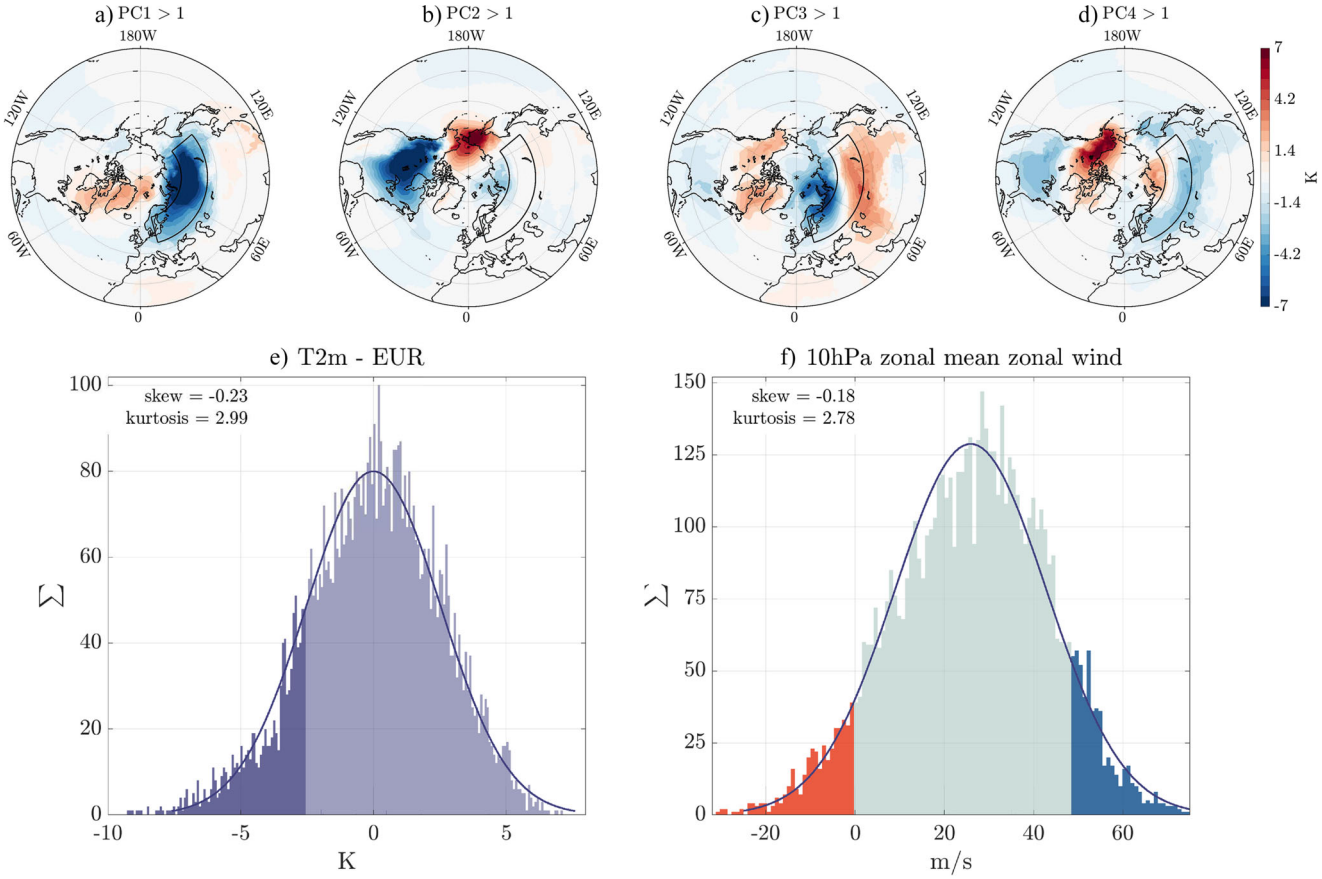

Fig. 1 a-d) Composite T2m anomalies based on days with standardized PC values > 1 of the first 4 modes of variability. Only significant values at the 1% level based on a two-sided t-test are shown. The black box indicates EUR. e) Histogram and corresponding probability density function of the Eurasian T2m index with darker blue values indicating days with T2m less than one negative standard deviation. f) Histogram of 10hPa zonal mean zonal wind index at 60°N. SSW and SPV days are marked in red and blue, respectively

first event day. If the last day of one event and the first day of the following event are less than 5 days apart and, additionally, the T2m anomaly does not increase to -0.25 standard deviations, the events are counted as one, yielding 58 events in total. No major changes of the overall results occur when varying these two conditions slightly.

The strength of the stratospheric polar vortex is evaluated using the 10hPa zonal mean zonal wind at 60°N as an index shown in Fig. 1f, whose distribution is slightly flat (kurtosis: 2.78) and negatively skewed (skewness: -0.18). The onset day of an extreme stratospheric vortex is taken when the zonal mean wind turns easterly, commonly associated with a sudden stratospheric warming (SSW), or exceeds 48m/s, i.e. a strong stratospheric polar vortex (SPV).

The cold events at the surface are divided into different groups depending on the occurrence of a stratospheric vortex event in the 40 days prior to their onset. Thus, we classify 39 neutral, 9 SSW PCEs, and 11 SPV PCEs that are listed in Table 1 including the date of the stratospheric event (first column), time to PCE (second column), date of PCE (third column) and length of PCE (fourth column). Note, that one of the events (06.03.1980) is counted as both SPV PCE and SSW PCE and two of the SSW PCEs share the same detected stratospheric signal prior to their onset. The type of SSW events (vortex split (S) or vortex displacement (D)) evaluated by Hall et al. (2021) have been matched with the detected SSW onset days in this study (Table 1b; fifth column). Among the detected SSW PCEs are 5 vortex split and 3 vortex displacement events. Mitchell et al. (2013) and Kretschmer et al. (2018b), for example, find SSW associated with the latter type to induce unusually cold temperatures in North America while an exceptional cooling over Eurasia is rather associated with the former event type. However, Maycock and Hitchcock (2015) shows that the difference across responses is weak. Therefore, and additionally keeping the sample size of our study in mind, we have not further distinguished these two groups in the analysis.

Table 1 Detected SPV PCEs (a) and SSW PCEs (b)

(a) SPV				(b) SSW				
SPV	gap	PCE	length	SSW	gap	PCE	length	type
15.01.80	9	24.01.80	11	01.03.80	5	06.03.80	26	D
05.02.80	30	06.03.80	26	04.12.81	28	01.01.82	13	D
04.01.84	26	30.01.84	13	01.01.85	9	10.01.85	14	S
21.11.86	23	14.12.86	33	01.01.85	33	03.02.85	36	S
21.12.89	22	12.01.90	9	23.01.87	38	02.03.87	26	D
12.12.94	0	12.12.94	11	26.02.99	6	04.03.99	23	S
21.12.99	8	29.12.99	9	09.02.10	10	19.02.10	15	S
11.01.07	37	17.02.07	12	12.02.18	11	23.02.18	11	S
21.01.11	24	14.02.11	14	01.01.19	31	01.02.19	6	S
15.12.13	40	24.01.14	16					
29.12.17	21	19.01.18	6					

The gap (second column) between SPV/SSW date (first column) and PCE onset date (third column) as well as the length of the latter (fourth column) are given in days. The type of SSW is given in the fifth column in (b)

2.2.3 Statistical and Dynamical Analysis

The quantile regression (QR) model (Koenker and Hallock 2001) has been used to analyze trends in the distribution of extreme cold T2m anomalies corresponding to the lowermost quantiles 0.01 and 0.05 as well as the median for comparison. As described in Elsner et al. (2008), gridded fields of T2m anomalies are used as the response variable and time as the predictor variable.

Composites of various variables for SSW PCE and SPV PCE onset days as well as for negative and positive lags are analysed to expose common and distinctive characteristics and patterns. Significance at the 10% level is evaluated based on 10000 bootstrap samples (Efron and Tibshirani 1993) unless stated differently.

The Plumb-flux (Plumb 1985), a diagnostic tool allowing for the derivation of the three dimensional flux of wave-activity (WAF), is almost parallel to the group velocity and thus energy propagation of the flow in the slowly varying limit. The three dimensional vector is given by Eq. 1.

$$F = p\cos(\phi)\begin{pmatrix} \frac{1}{2a^2\cos^2\phi}\left[\left(\frac{\partial\psi'}{\partial\lambda}\right)^2 - \psi'\frac{\partial^2\Psi'}{\partial\lambda^2}\right] \\ \frac{1}{2a^2\cos\phi}\left[\frac{\partial\psi'}{\partial\lambda}\frac{\partial\psi'}{\partial\phi} - \psi'\frac{\partial^2\psi'}{\partial\lambda\partial\phi}\right] \\ \frac{2\Omega^2\sin^2(\phi)}{N^2a\cos(\phi)}\left[\frac{\partial\psi'}{\partial\lambda}\frac{\partial\psi'}{\partial z} - \psi'\frac{\partial^2\psi'}{\partial\lambda\partial z}\right] \end{pmatrix} \quad (1)$$

Here, p ($p/1000hPa$) is the pressure, ϕ and λ are latitude and longitude, a and Ω are the radius and rotation rate of the earth, N the Brunt-Vaisälä frequency, Ψ' the perturbation streamfunction and $z = -H\ln p$ the height with constant scale height H. Positive values of the vertical component correspond to upward propagating waves.

The vertical configuration of zonal stratospheric winds may provide for a reflective surface that redirects upward travelling planetary waves back down to the troposphere. The reflective state of the stratosphere can be evaluated by following the approach in Nath et al. (2014), who use the meridionally averaged (58°N-74°N) zonal wind to calculate the time evolution of the reflective index across longitudes with Eq. 2.

$$U_r = U2 - U10. \quad (2)$$

The stratosphere is reflective in case the zonal wind in 2hPa ($U2$) is less than in 10hPa ($U10$), i.e. negative U_r.

3 Results

3.1 Persistent Eurasian Cold Spells

Using QR to evaluate trends in gridded T2m anomaly fields with a focus on extremely cold EUR temperatures, we find that for the 0.01 (Fig. 2a) and 0.05 (Fig. 2b) quantiles, the most eastern and most western parts of the study region show a positive trend that is substantially higher than what the median QR (Fig. 2c) suggests. A negative trend stronger than $-0.1K/yr$ centered between 50°E and 85°E in case of the 0.01 quantile, and up until $-0.05K/yr$ at around 85°E for the 0.05 quantile indicates that extremely cold temperatures have become colder over the last decades. Increasing extremely cold and mean temperatures over vast areas over the Arctic Ocean, may have impacts on the Arctic Sea ice and thus cold temperatures over EUR. Figure 2d shows a composite of the 58 identified EUR PCEs. The coldest T2m anomalies cover the central area of EUR,

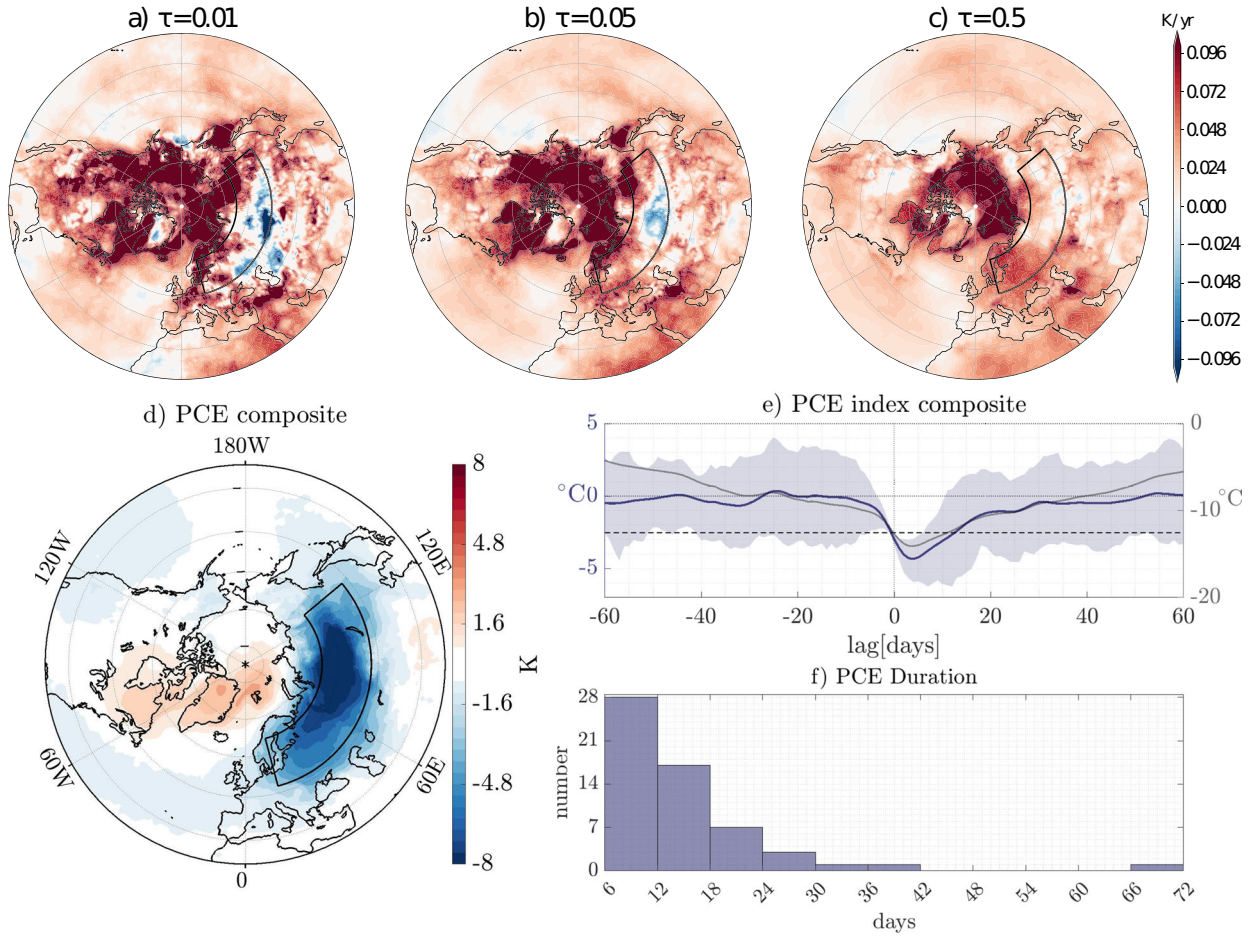

Fig. 2 a-c) QR of T2m for $\tau = [0.01, 0.05, 0.5]$. d) T2m anomaly composite based on all PCEs. e) Lagged T2m anomaly index composite (blue; left-hand y-axis) including 90% confidence interval and T2m absolute value index composite (grey; right-hand y-axis). f) Histogram of PCE's durations

exceeding -8K and, interestingly, partly overlap with the region covered by the negative QR coefficients for the 0.01 and 0.05 quantile. The composite time evolution of the EUR T2m anomaly (absolute value) index for 60 days before to 60 days after the onset is shown as the blue (grey) line in Fig. 2e, including the 90% confidence interval as shading, to analyse the extent and change of intensity of PCEs with time. The dashed line indicates the threshold of one negative standard deviation corresponding to the T2m anomaly index. On average the T2m drops to negative anomalies about 10 days before, reaching peak absolute values of about -13°C with anomalies remaining negative until 50 days after the PCE onset. Note that the index is not significantly different from zero when the confidence interval overlaps the zero line, which is the case between -3-days to +10-days lag. This can partially be reasoned by varying duration among the PCEs, shown in a Histogram in Fig. 2f. We find that 28 PCEs last between 6 and 11 days, another 17 between 12 and 17 days and 7 events between 18 and 23 days. Further, three PCEs are longer than three weeks, i.e. between 24 and 29 and another three even longer than one month with one being exceptionally long-lasting starting on the 8th December 2009 until the 12th February 2010, i.e. 67 days.

3.2 Characteristics Depending on the Stratosphere

Following the bottom-up perspective, we group the PCEs depending on whether they are preceded by an SPV (11 events), SSW (9 events) or a neutral state in the stratosphere (39 events) to evaluate differences across groups. Figure 3a shows the distribution of PCE's by month. In total, most PCEs develop in December (14) and January (13), followed by November (12), March (10) and lastly February (9) with the least amount of detected PCEs. More SPV PCEs occur during December and January compared to February and March. In contrast, during February and March SSW PCEs are more common than during December and January. Interestingly, in February, PCEs are more common to emerge after an SSW event than a neutral state of the

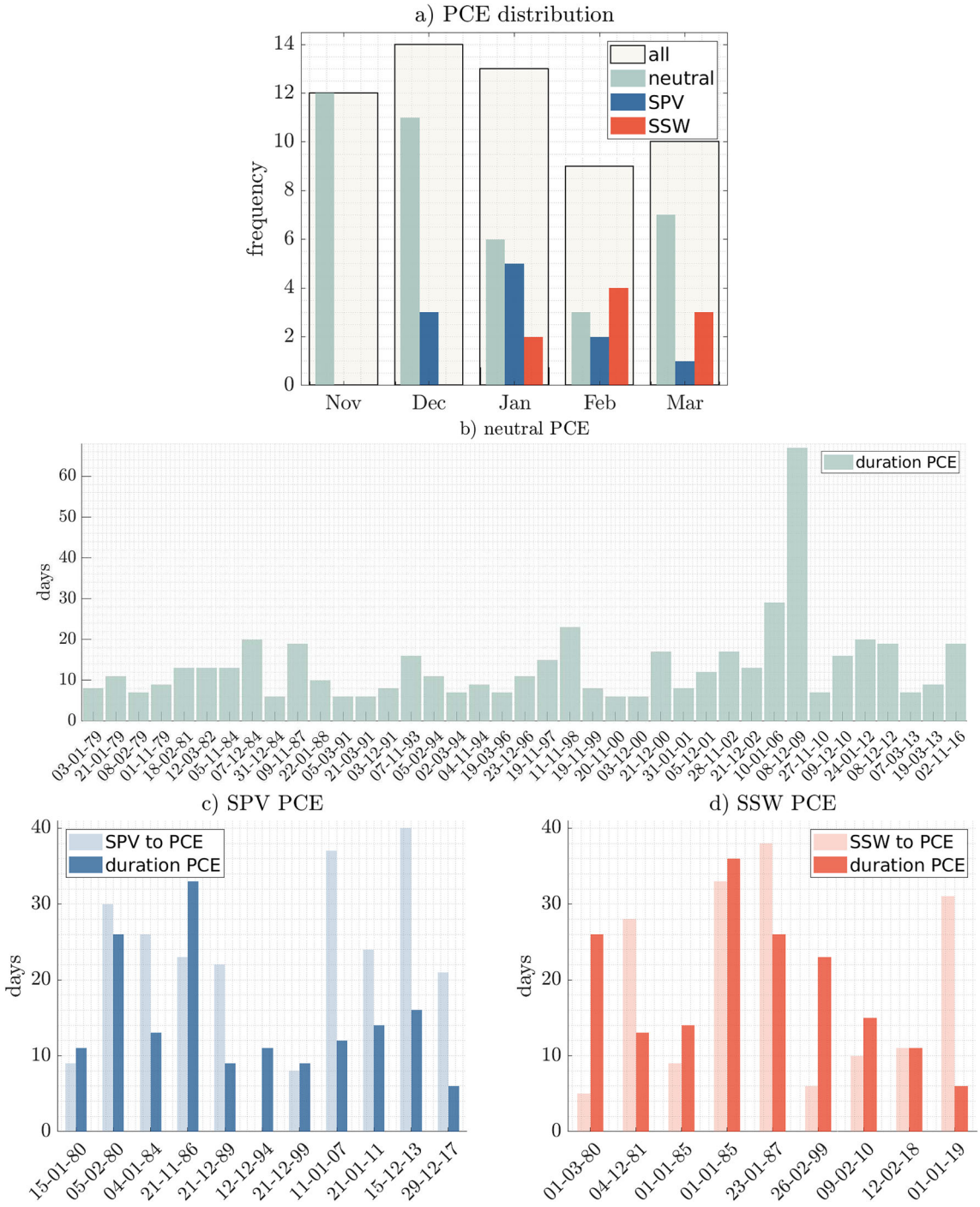

Fig. 3 a) Occurrence distribution of neutral (green), SPV (blue) and SSW (red) PCEs across months. b) Duration of neutral PCEs., where x-axis indicates start of PCE. c) Time interval between stratospheric signal and PCE (transparent blue) and duration of PCE (solid blue) for SPV PCEs, the x-axis indicates the date of initial stratospheric signal. d) same as c) but for SSW PCEs

stratospheric polar vortex. The decrease in neutral PCEs during January and February may be explained by the evolution of the stratospheric polar vortex, i.e. the spin up of strong zonal westerlies in the beginning of the winter, the most active phase during mid-winter and the weakening during the end of the season when sunlight returns to the high-latitude stratosphere.

PCEs can thus occur during the full range of stratospheric variability. In the following we show common and distinct characteristics of each group. The duration of neutral PCEs

from the first day of detection (x-axis) is given in Fig. 3b. Of 39 events in total, 18 are shorter than or equal to 10 days, 18 between 10 and 20 days and 3 events longer than 20 days. Consistent with the overall positive trend in outer quantiles over Eurasia (see e.g. Fig. 2b), fewer events are detected during the second half of the time series, i.e. between 1999-2019. Similarly, for SSW PCEs (SPV PCEs) we find 6 (7) events in the first and 3 (3) in the second half of the time series. In the following, we focus on SPV PCEs and SSW PCEs. An analysis of neutral PCEs can be found in the supplementary information. Figure 3c shows the time between SPV and the onset of the PCE (transparent) and the duration of the corresponding PCE (solid color). Here, the date on the x-axis marks the day of the initial stratospheric SPV signal. Three PCEs start within 10 days after a SPV, which then last around 10 days. Six PCEs start between 20 and 30 days after a SPV with durations ranging between 6 and 33 days. Lastly, two PCEs begin after 37 and 40 days after a SPV, lasting for 12 and 16 days, respectively. Figure 3d shows the same as Fig. 3c but for PCEs following SSWs. Within 11 days after an SSW event, 5 PCEs have been detected that have durations between 11 and 26 days. The remaining 4 PCEs developed 4 to around 5.5 weeks after an SSW of which two last less than 2 weeks and two longer than three weeks.

Noticeably, 8 out of 11 SPV PCE events start more than 20 days after the stratospheric signal while in case of SSW PCEs 5 out of 9 start no later than 11 days after the stratospheric signal.

3.3 Evolution

In the next step, we investigate differences in the evolution of extent and intensity of SSW PCEs and SPV PCEs with time. Figure 4a-b show a lagged composite of the EUR T2m anomaly (absolute value) index from 60 days before to 60 days after the onset day as the coloured (grey) line including its 90% confidence interval as shading. In case of SPV PCEs (Fig. 4a), the T2m index is mainly above average until about 5 days before the PCE onset. Thereafter, the T2m index is below one standard deviation for about 10 days and below the mean for almost one month. At higher lags, the T2m index is mostly above the mean. Further, the composite temperature anomalies drop to more negative values for SPV PCEs than SSW PCEs (Fig. 4b) corresponding to around -15.5°C for the former and around -13.5°C for the latter case. In case of SSW PCEs, the T2m index is lower than its mean the entire period before the drop below one standard deviation. While overlapping with the zero line, the confidence interval, noticeably decreases between around

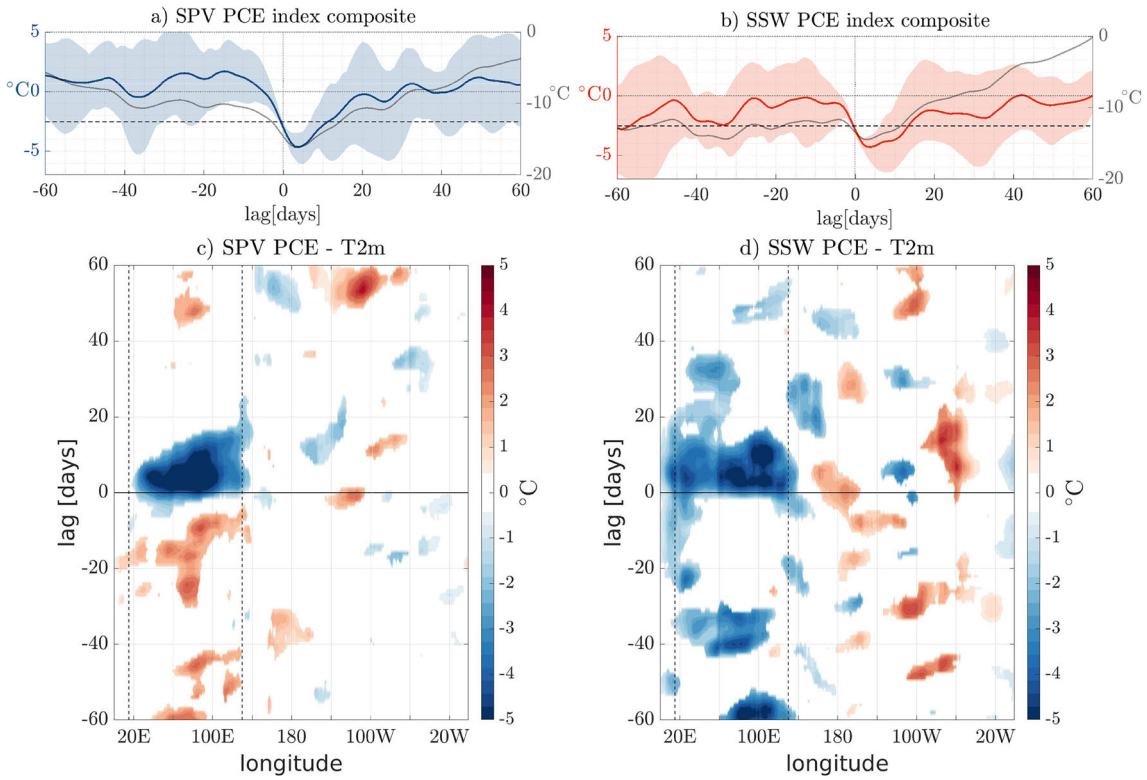

Fig. 4 Lagged T2m anomaly index composite (coloured; left-hand y-axis) including 90% confidence interval and T2m absolute value index composite (grey; right-hand y-axis) for SPV PCEs (a) and SSW PCEs (b). Lagged evolution of T2m anomalies meridionally averaged over the study area for SPV PCEs (c) and SSW PCEs (d)

40 and 33 days before the PCE. On average, the T2m stays lower than the PCE threshold for around 15 days, lower than its mean for 40 days, and mostly afterwards.

Further investigating the longitudinal evolution from -60-days to +60-days lag, composite T2m anomalies, latitude-weighted and meridionally averaged over the study region, are shown in Fig. 4c-d. Vertical dashed lines mark the zonal borders of the study region. Only significant values are shown. In case of SPV PCEs (Fig. 4c), we find positive anomalies to prevail across EUR for negative lags. Further, from 0-days to +10-days lag, negative T2m anomalies are most dominant in the central part. The eastward tilt of the anomaly pattern may hint at an eastward propagation of the anomalies. Thus, the farther east in the study region, the longer the negative anomalies persist, ranging between less than 10 days on the western side to almost 20 days on the eastern side. In contrast, for SSW PCEs (Fig. 4d), we find negative T2m anomalies in eastern EUR around 60 days and in the central part around 30 to 40 days before the PCEs start. Further, at about 20 days before the PCE onset, significant negative anomalies develop in western EUR. During the PCE, while anomalies in eastern EUR are colder, the ones on the western side are more persistent (up until +20-days to +25-days lag) with a slight eastward propagation.

Figure 5 shows SPV PCE composite anomalies for -10-days, -5-days, 0-days, +5-days and +10-days lag (left to right) for T2m (first row), SLP (second row), z500 (third row) and 250hPa zonal wind (u250) (fourth row). Only significant anomalies are shown. Positive T2m anomalies in the central eastern part accompanied by negative SLP anomalies in the center of the study area emerge 10 days before the PCE onset (first column). At the same time, a z500 wave train stretches from North Africa to the

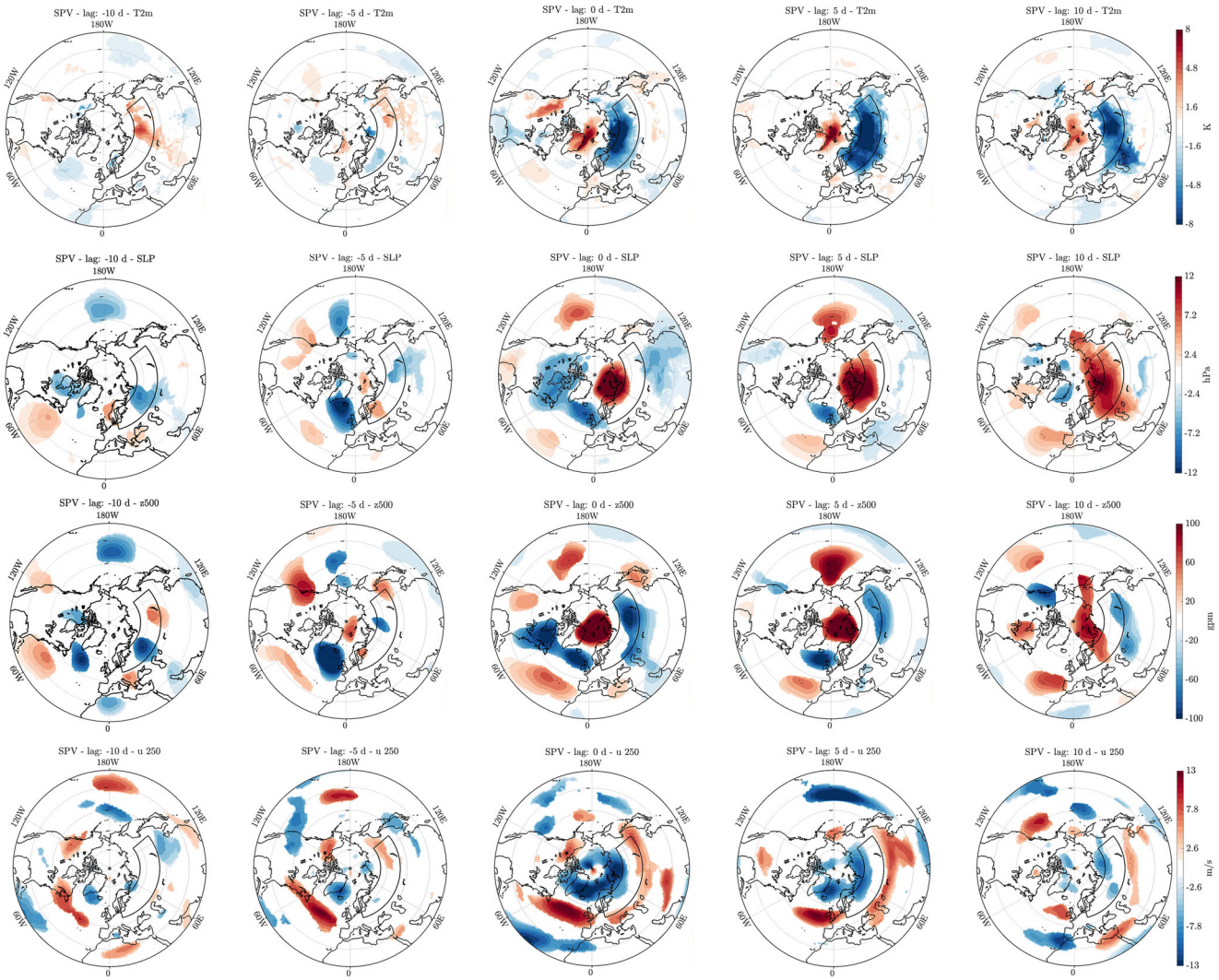

Fig. 5 Lagged composite T2m (first row), SLP (second row), z500 (third row) u250 (fourth row) anomalies for -10-days, -5-days, 0-days, +5-days and 10-days lag (left to right) relative to the onset of SPV PCEs. Only significant anomalies are shown

eastern part of the study region. Further, we find negative (positive) z500 and SLP anomalies over the southern tip of Greenland (western North Atlantic), accompanied by accelerated central North Atlantic u250. Five days before the event (second column), positive T2m anomalies in the study region fade while negative ones develop over its western half. The North Atlantic height anomalies merge with the Rossby wave train found at -10-days lag with positive (negative) z500 centers over the eastern and western (central) part of EUR. At 0-days lag (third column) we see a strong zonal acceleration of the u250 over the North Atlantic and the southern border of the study area. Further, the positive heights over the Arctic Ocean expand with positive SLP coinciding with negative T2m over central northern EUR. Strong positive T2m anomalies develop over the Arctic Ocean in the Barents sea area that fade at +10-days lag (fifth column). From the 0-days to +5-days lag (fourth column) we find a slowly eastward propagating wave. Together with positive SLP over EUR, the negative T2m anomalies in the study region strengthen and expand at +5-days lag. A zonal shift of T2m at +10-days lag, covering particularly the central and eastern part of EUR, reflect the eastward tilt identified in Fig. 4c.

For SSW PCEs, the pattern evolution is shown in Fig. 6. At -10-days lag (first column), we do not find significant T2m anomalies in most parts of EUR except for the far west. The latter negative anomalies are accompanied by positive (negative) SLP and z500 anomalies over Iceland (central Europe). Five days later (second column), negative T2m anomalies develop north of the northern border as well as the western part of the study region. Positive SLP and z500 anomalies strengthen and extend further toward EUR. Additionally we find a positive z500 anomaly over the Ural region as well as two negative ones on the most western and most eastern sides of EUR. Together with negative SLP anomalies over the central North Atlantic,

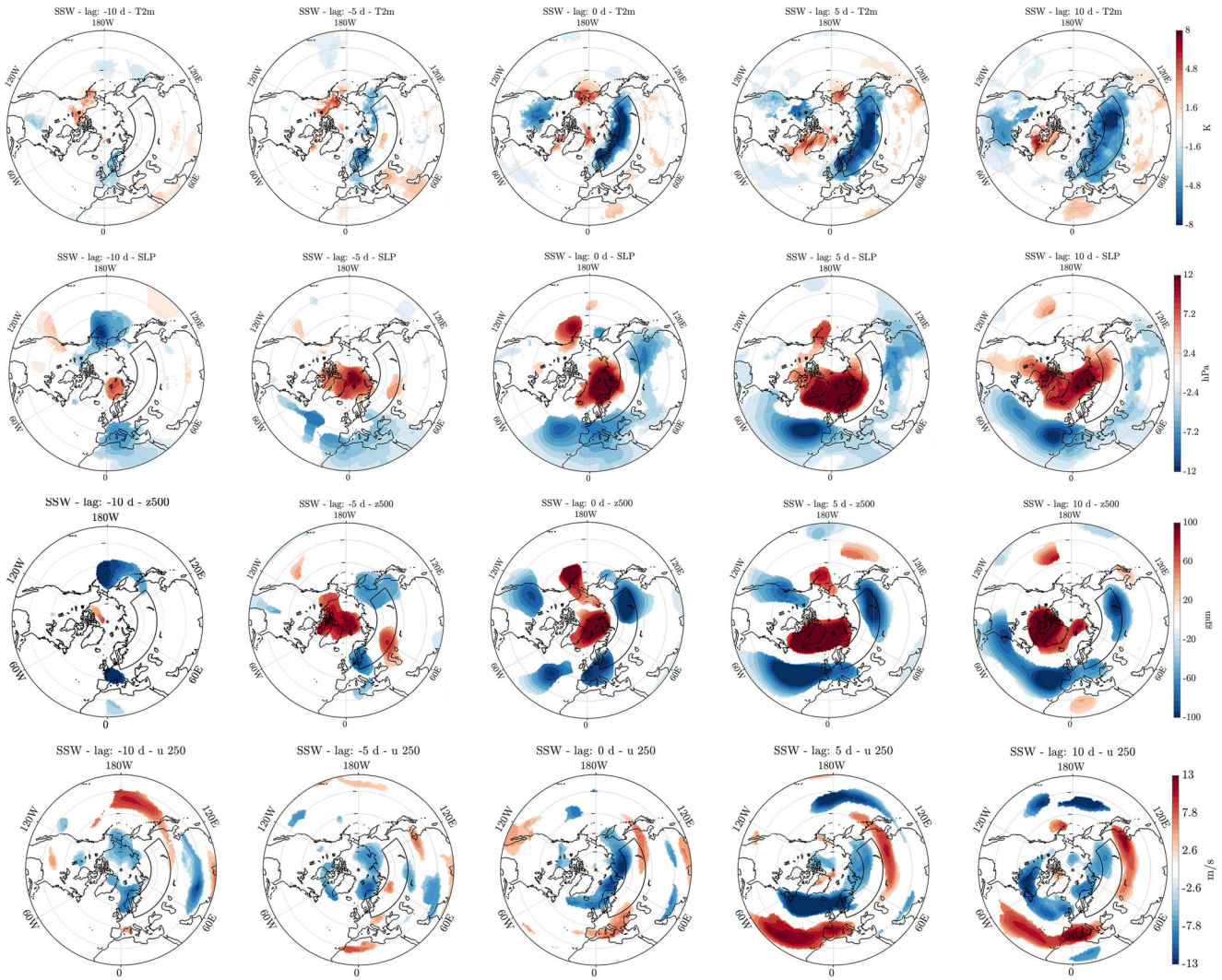

Fig. 6 Same as Fig. 5 but for SSW PCEs

both negative SLP and z500 anomalies over central Europe and eastern EUR as well as positive z500 over the Arctic Ocean strengthen at 0-days lag and are accompanied by a southward shift of the jet (third column) that coincides with negative z500 anomalies over EUR. Concurrent T2m anomalies stretch across northern EUR before moving further south, covering almost the entire study region 5 days later (fourth column) with particularly strong values over its central part. Concomitantly, a negative NAO signature in SLP and z500 together with a southward shift of the jet stream is visible over the North Atlantic at +5-days and +10-days lag (fourth and fifth column). The latter can be additionally observed over eastern EUR. With increasing lag, the positive SLP anomalies together with the center of strongest negative T2m anomalies migrate further toward the eastern part of Eurasia.

Concluding, in both cases, the T2m anomalies affect the whole study region but set in more abruptly in the SPV PCE case. Further, a strong positive quasi-stationary z500 anomaly with a barotropic structure develops over the Arctic, yielding a southward shift of the jet over Eurasia and thus blocking warm air advection from the South, thus facilitating the PCE. In the SSW PCE case, Ural blocking is present before the PCE onset and the Arctic anticyclonic anomaly is connected to positive z500 anomalies over Greenland related to the negative NAO phase. In contrast, co-located with warm T2m anomalies, the positive z500 anomaly over the Arctic is included in a zonally propagating Rossby wave train originating in the North Atlantic in the SPV PCE case.

3.4 The Stratospheric Link

In the next step we want to see how and if the stratosphere can be linked to the PCEs. On that account, composites of latitude-weighted geopotential heights and temperature anomalies averaged over all grid points between 60°N and 75°N in the former as well as north of 70°N in the latter case are shown in Fig. 7a-d.

For SPV PCEs (Fig. 7a) we find significant negative height anomalies in the upper stratosphere from around -25-days lag. A downward migration of the signal is observed but the tropopause is not crossed before about 30 days after the PCE. However, the signal reaches the approximate tropopause level (horizontal line) close to 0-days lag. Similarly, we see downward progressing cold polar cap temperature anomalies (Fig. 7c) from around -35-days to 0-days lag that pass the tropopause only at around -20-days lag. Interestingly, we find positive anomalies in the troposphere and surface around the onset of the SPV PCEs that likely reflect the near surface warming over the Barents sea (Fig. 5; first row).

In case of SSW PCEs (Fig. 7b), significant positive geopotential height anomalies are observed from about -20-days lag. A downward migration of this signal is clearly visible, reaching the surface at about -20-days lag as well as between -5-days and +10-days lag. This is consistent with the development of the negative phase of the NAO, visible in Fig. 6. Additionally, a warming over the polar cap, identified at around -20-days lag, progresses downward into the troposphere but without significant connection to the surface (Fig. 7d).

In the right constellation, the lower stratosphere can be in a reflective state, i.e. instead of being absorbed, upward traveling planetary waves are reflected back to the troposphere where they accumulate and influence the circulation. Following Nath et al. (2014), we calculated the reflective index of the stratosphere as a function of longitude and time (Fig. 7e-f) with negative values indicating that reflection is possible. Only significant values are shown. In the SPV PCE case (Fig. 7e), the stratosphere is significantly non-reflective from across most longitudes from -20-days to +20-days lag except between around 100°W to 140°W. Across the latter longitudes, the stratosphere is dominantly reflective up until +5-days lag. In contrast, in case of SSW PCEs (Fig. 7f), we only find significant positive values across most longitudes and lags indicating prominent wave absorption. However, before the PCE onset, values are dominantly non-significant.

To further investigate upward and downward propagation of planetary waves, Fig. 8 shows the latitude-weighted and then averaged between 58°N and 74°N vertical WAF component (shading) as well as WAF in the x-z domain (arrows) across longitudes for -10-days, -5-days, 0-days, +5-days and +10-days lag (from top to bottom) for SPV PCEs (left column) and SSW PCEs (right column). The vectors are scaled with 15 and 0.5 in the x and z direction, respectively. Consistent with the reflective index, we indeed find downward reflected waves between about 120°W to around 55°W for -10-days to +5-days lag for the SPV PCE case that converge with upward directed waves in the mid- to upper troposphere, thereby piling up energy and thus potentially influencing the North Atlantic circulation. A minor downward WAF at similar location but spatially limited is found for SSW PCEs at -5-days lag. In both cases, upward wave propagation into the stratosphere is prominent over eastern EUR and the Pacific.

The horizontal distribution of absolute values and anomalies of the 3D WAF with vertical component as shading and horizontal component (x-y) as arrows at 500hPa (first and second column) and 150hPa (third and fourth column) composited for SPV PCEs at -10-days, -5-days, 0-days, +5-days and +10-days lag (top to bottom) is shown in Fig. 9.

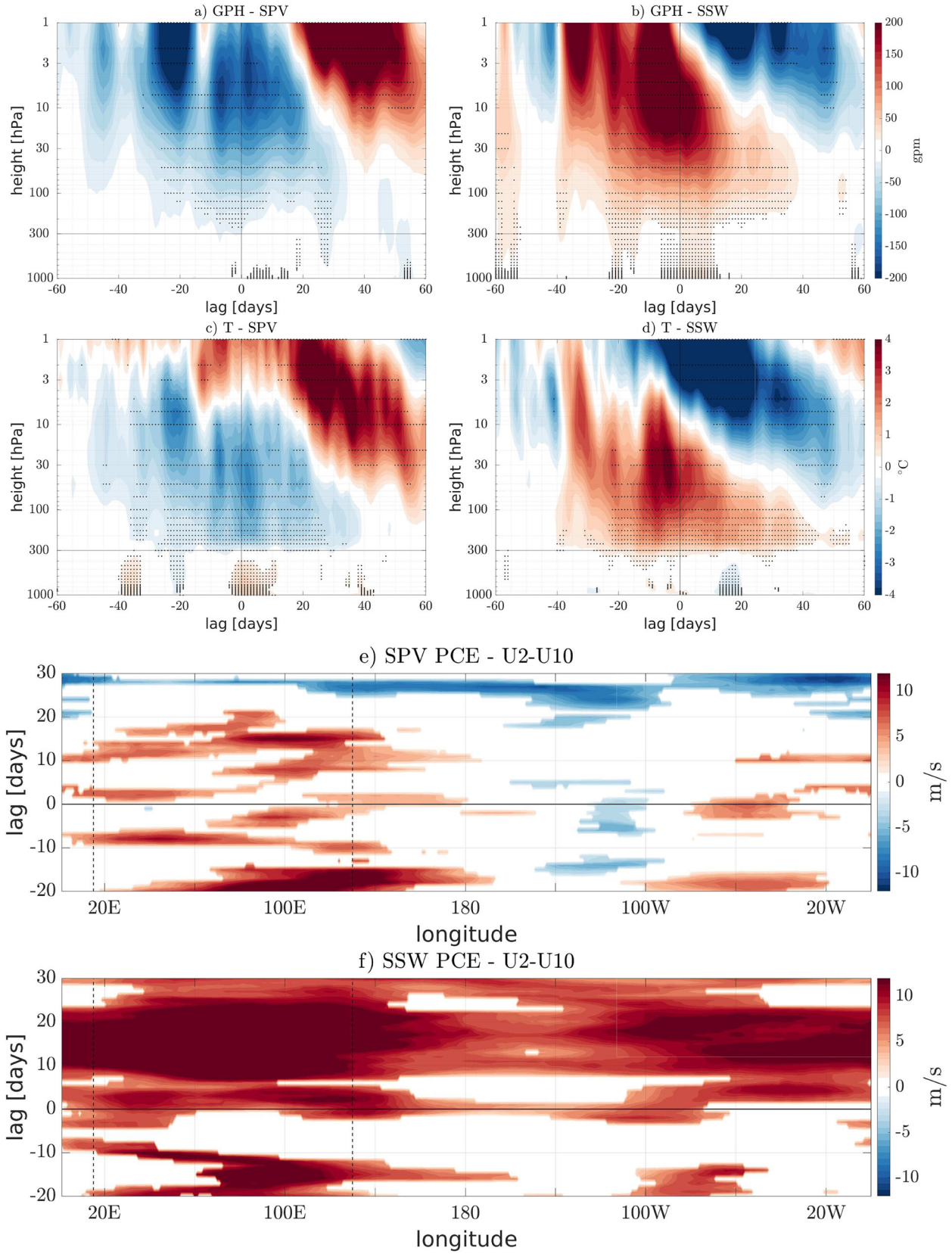

Fig. 7 a,b) Zonal mean geopotential height (averaged between 60°N-75°N) and c,d) polar cap temperature anomalies (averaged between 70°N-90°N) for SPV PCE (left column) and SSW PCE (right column) for -60-days to +60-days lag. Horizontal black line marks the approximated tropopause level. Reflective index U_r for SPV PCEs (e) and SSW PCEs (f) for -20-days to +30-days lag

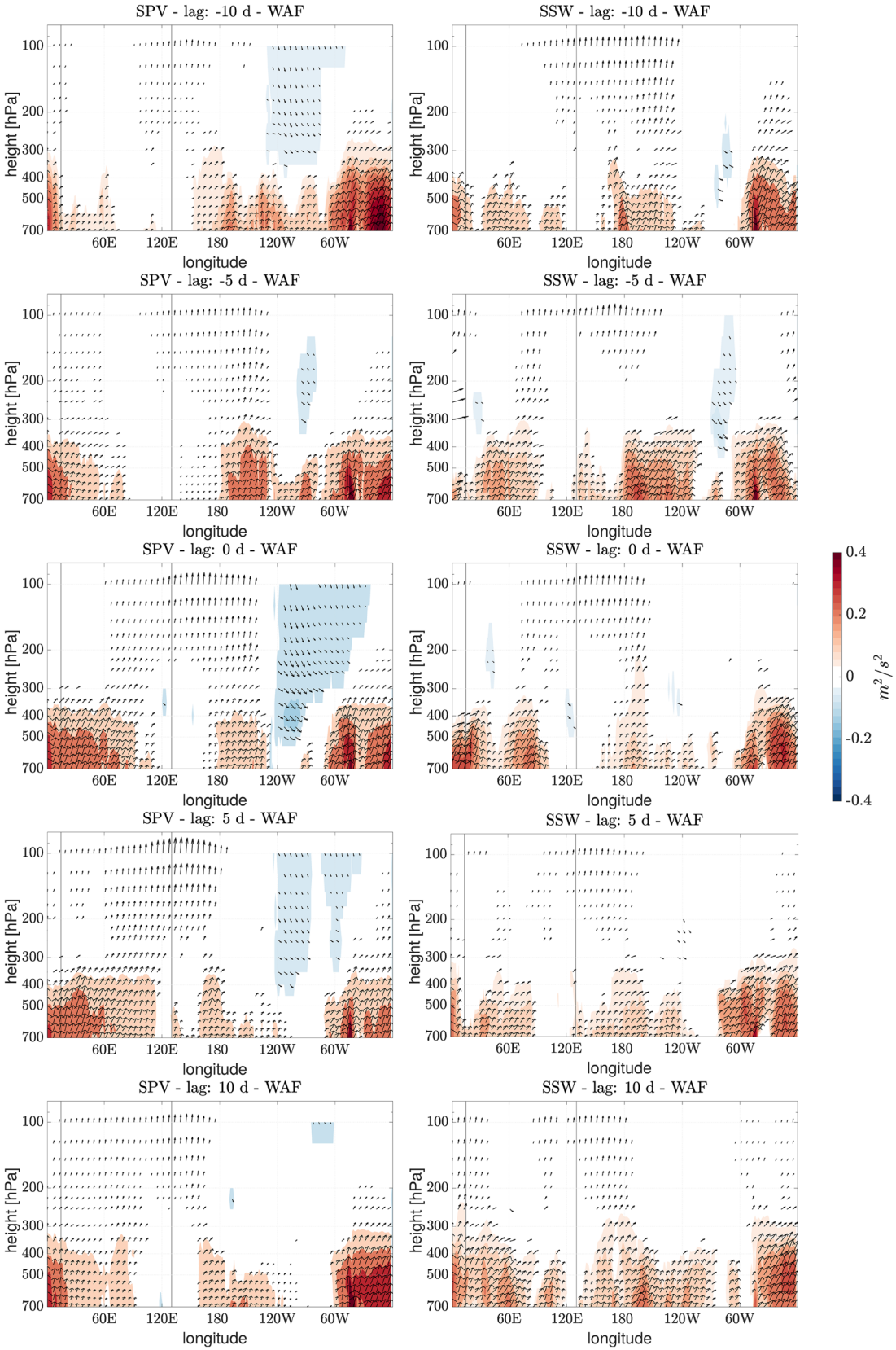

Fig. 8 Latitude-weighted average of wave activity flux (58°N-74°N) for -10-days, -5-days, 0-days, +5-days and +10-days lag (top to bottom) for SPV PCEs (left column) and SSW PCEs (right column). Shading shows the vertical component (z) while arrows indicate the vertical (x-z) domain of WAF. Vertical black lines indicate the study region

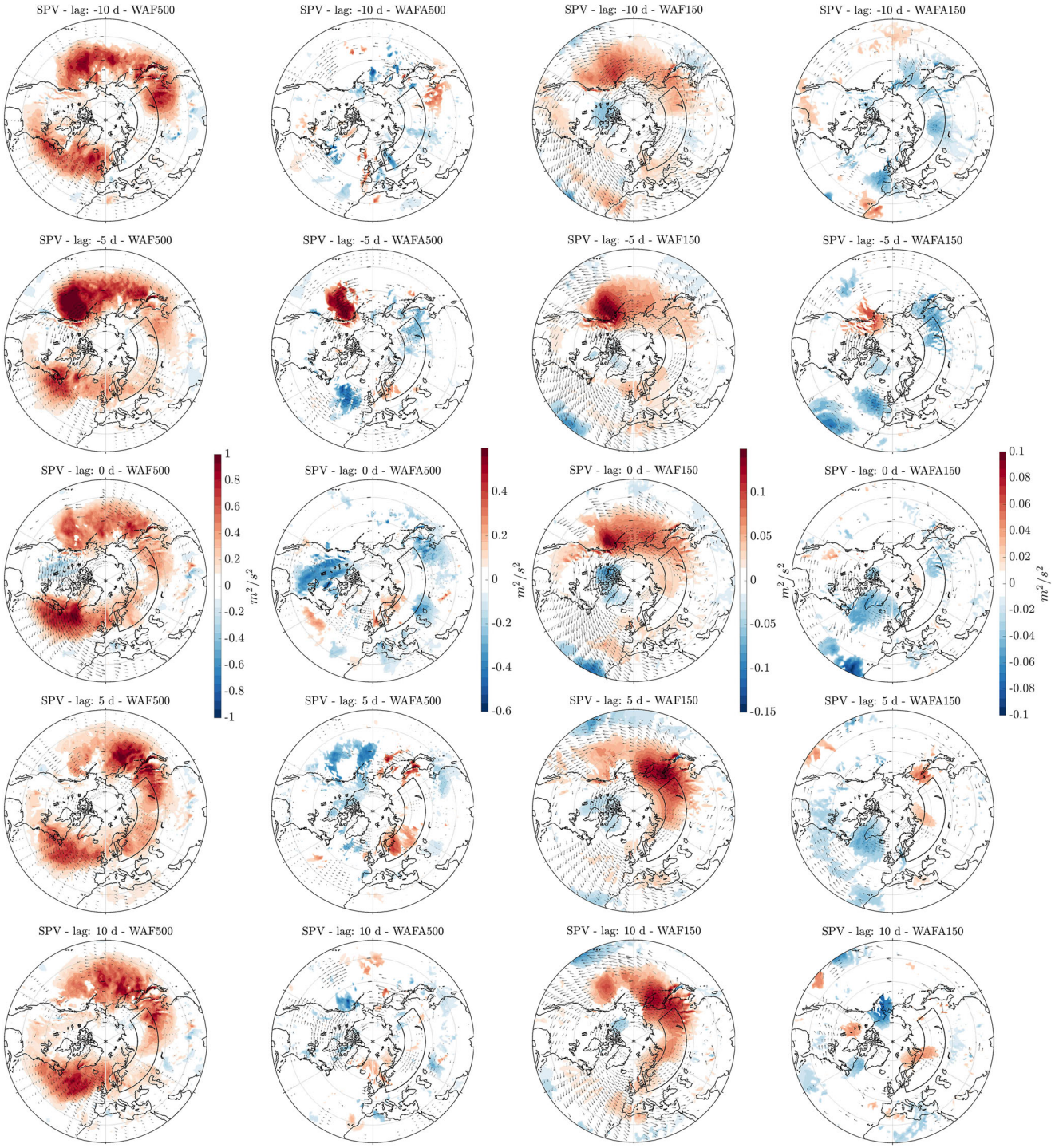

Fig. 9 Absolute values and anomalies of the vertical (shading) and horizontal (arrows) component of WAF in 500hPa (first and second column) and 150hPa (third and fourth column) for SPV PCEs -10-days, -5-days, 0-days, +5-days and +10-days lag (top to bottom). Only significant values are shown

At -10-days to -5-days lag, stationary waves dominantly propagate up- and, between 30°N and 60°N southeastward over East Asia, the North Pacific and western North America in both heights, as well as over the North Atlantic in 500hPa, which is particularly more (less) than usual over the Gulf of Alaska (Central North Atlantic and eastern Siberia/EUR) at -5-days lag. Western EUR experiences unusually strong upward wave propagation in 500hPa from -5-days to +5-days lag. Additionally, we find an eastward flux over EUR, the Aleutians and several zonal stretches

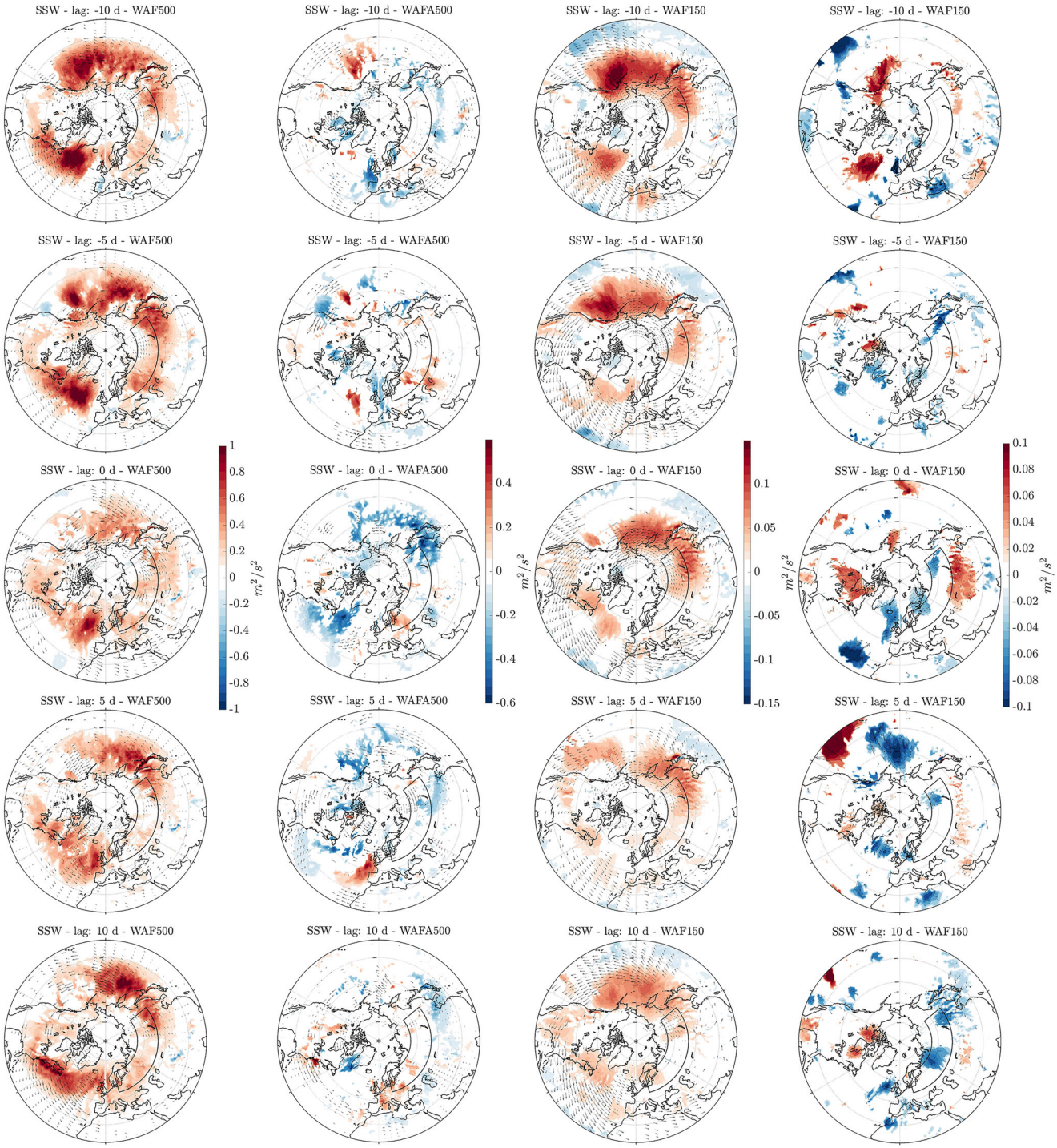

Fig. 10 Same as Fig. 9 but for SSW PCEs

between 60°N and 75°N for both heights and throughout the analysed lags. Interestingly, the North Atlantic eastward flux is unusually weak from -5-days to +5-days lag which may hint at slower than usual eastward propagating Waves. At -5-days, we see unusually strong eastward fluxes, locally confined over the Barents sea, towards the region covered by the anticyclonic anomaly. In 150hPa, negative WAF anomalies, i.e. downward propagating waves, are found over northern Canada and Greenland between -10-days lag to +5-days lag. At 0-days lag, unusually strong down- and eastward directed North American WAF appears in 500hPa, seemingly part of a wave train with alternating positive and

negative vertical WAF anomalies over the North Atlantic. Concurrently, upward directed anomalous WAF over central (150hPa) and western (500hPa) EUR strengthens.

Figure 10 shows the same as Fig. 9 but for SSW PCE events. At -10-days to -5-days lag, we find unusual upward propagating stationary wave over the central east Pacific, and, different to the SPV PCE case, over the North Atlantic in both heights. At the same time, southeastward directed WAF are found over the North Atlantic and central east Pacific while eastward wave propagation is found between about 55°N to 75°N and 90°E to 90°W. At -5-days and 0-days lag, we find negative (positive) vertical WAF anomalies at 150hPa (500hPa) over western EUR. From 0-days to +5-days lag, upward directed WAF over eastern EUR is unusually weak in both heights. Simultaneously, upward directed WAF over the central (both heights) and western (500hPa) North Pacific is unusually weak. Positive (negative) WAF anomalies are found at 500hPa (150hPa) over the eastern North Atlantic at +5-days lag (+5-days and +10-days lag). Simultaneously, eastward wave propagation over Northern Europe is unusually weak. At +10-days lag positive vertical WAF anomalies over Canada and negative anomalies over central EUR emerge at 150hPa while at 500hPa weak (unusually strong) upward wave propagation over Southern Greenland (central Europe and Central to eastern North America) appears.

Concluding, in the SPV PCE case, we find a reflective stratosphere over the eastern US consistent with downward high-latitude wave propagation converging in the mid-troposphere as well as downward propagation over the central North Atlantic of which the latter is co-located with positive height anomalies included in the wave train slowly propagating toward EUR and unusually strong eastward wave fluxes over the Barents sea before the PCE onset. For SSW PCEs we find the upper stratosphere to be mainly non-reflective but with downward wave propagation from the lower stratosphere that is at similar location but weaker as in the SPV PCE case.

4 Discussion and Conclusion

The negative impacts of PCEs make their early prediction, preferably on S2S-timescales, a necessity researchers are striving for. The study region EUR is chosen as it overlaps with the area with highest explained variability of T2m across the Northern Hemisphere based on an EOF analysis of daily winter-time data. Central EUR T2m extremes show a decreasing trend, i.e. more than -0.1°/yr, based on QR using low quantiles that cannot be identified using the median. This trend, together with a concomitant positive trend over the Barents/Kara sea is consistent with previous studies linking sea ice loss and related reduction in meridional temperature gradient (e.g. Outten and Esau 2012) to blocking over and cold air advection toward EUR (e.g. Mori et al. 2014; Yao et al. 2017).

The T2m index, as a latitude-weighted average across EUR, is negatively skewed, indicating the recurrent presence of extreme cold events. Based on the stratospheric state in the 40 days before their onset, we find PCEs to occur during the full range of stratospheric variability, but SPV PCEs dominate in December/January and SSW PCEs in February/March. Conspicuously, 8 out of 11 SPV PCEs start more than 20 days after the initial stratospheric signal in 10hPa while 5 out of 9 SSW PCEs start no later than 11 days after. In both cases, the T2m anomalies affect the whole study region, but SPV PCEs are colder and set in more rapidly after a period of above average T2m. In contrast, EUR is exposed to unusual cold T2m before SSW PCEs set in. Consistent with the AO response given in (e.g. Kim and Son 2016), coldest anomalies are located along the northern border of EUR during the onset of SSW PCEs, which then migrate eastward. Negative anomalies, however, are most persistent in western EUR. Contrariwise, SPV PCEs endure longest in eastern EUR during their evolution.

In both cases, a strong positive, quasi-stationary z500 anomaly with a barotropic structure over the Barents/Kara sea and northern Siberia and a downstream negative anomaly in mid-latitudes yields a southward shifted jet stream over EUR, thereby, inhibiting (promoting) warm (cold) air advection from the South (North). The remote link to the North Atlantic, however, differs across SSW and SPV PCEs. In the former case, we find this anticyclonic anomaly to be connected to positive heights over Greenland as part of the negative NAO phase progressing downward from the stratosphere, reaching the surface 5 days before the PCE onset. Simultaneous unusually weak eastward wave fluxes over Northern Europe and Ural blocking are likely to be involved in generating the cold temperatures. In contrast to absorbing upward traveling planetary waves in the SSW PCE case, the stratosphere is reflective over the North American sector before SPV PCE events. Stratospheric reflection is consistent with geopotential height and polar cap temperature anomalies not progressing into the troposphere (Perlwitz and Harnik 2004). Upward propagating planetary waves over the Aleutians are reflected toward the western North Atlantic, where they converge with upward propagating waves in the mid-troposphere. Subsequent accumulation of wave energy potentially influences the tropospheric circulation (e.g. Perlwitz and Harnik 2004). We further find locally confined, unusually strong eastward wave fluxes into the Barents sea anticyclone. The latter is connected to a slowly propagating zonal Rossby wave train whose North Atlantic origin is approximately co-located with negative vertical WAF anomalies. While local, tropospheric processes can generate

the negative height anomalies over the Barents/Kara sea (Inoue et al. 2012), the above results suggest a remote influence in the sense of stratospheric wave reflection toward the North Atlantic and a subsequent modulation of z500 anomalies upstream of the Arctic anticyclone that act to reinforce the latter. Previous studies congruently linked the North Atlantic circulation with blocking over the Eurasian sector (e.g. Luo et al. 2016; Chen et al. 2021; Murto et al. 2022). While differing in exact location but consistent with our study, Luo et al. (2016) and Chen et al. (2021) link North Atlantic negative height anomalies and intensified wind speeds, as found in the present study, to the slowly eastward propagation of a Rossby wave train including an anticyclonic anomaly over EUR. Further, we find concomitant warming over the Barents Sea region and weakening of the mean westerly flow over northern EUR to be coherent with findings by Yao et al. (2017), who connect a reduced meridional temperature gradient to decreased Eurasian wind speeds and thus increased stationarity and persistence of the anticyclonic anomaly that is linked to EUR cold extremes.

Concluding, SSW PCEs and SPV PCEs have distinct and common local characteristics and remote influences. In both cases, the ascertained link to winter-time variability of the stratospheric polar vortex provides potential to enhance their extended-range predictability.

Supplementary Information The online version contains supplementary material available at https://doi.org/10.1007/s13143-022-00308-y.

Acknowledgements We acknowledge the European Centre for Medium Weather Forecasting, ECMWF, for providing the ERA5 reanalysis. The computations and data handling were enabled by resources provided by the Swedish National Infrastructure for Computing (SNIC) at the National Supercomputer Centre (NSC), partially funded by the Swedish Research Council through grant agreement no. 2018–05973. This research is supported by a faculty-funded PhD program. T. Hirooka was funded by International Meteorological Institute (IMI) of Stockholm University, Stockholm Sweden, and he was also supported by KAKENHI Grant numbers JP20H01973 and P18H01280. We thank two anonymous reviewers for their constructive feedback.

Funding Open access funding provided by Stockholm University.

Declarations

Competing interests The authors have no competing interests to declare that are relevant to the content of this article. We declare no conflict of interest.

References

Baldwin, M.P., Dunkerton, T.J.: Propagation of the Arctic Oscillation from the stratosphere to the troposphere. J. Geophys. Res. Atmos. **104**(D24), 30,937–30,946 (1999). https://doi.org/10.1029/1999JD900445

Baldwin, M.P., Dunkerton, T.J.: Stratospheric harbingers of anomalous weather regimes. Science **294**(5542), 581–584 (2001). https://doi.org/10.1126/science.1063315

Barnett, T.P., Heinz, H.D., Hasselmann, K.: Statistical prediction of seasonal air temperature over Eurasia. Tellus A: Dyn. Meteorol. Oceanogr. **36**(2), 132–146 (1984). https://doi.org/10.3402/tellusa.v36i2.11476

Charney, J.G., Drazin, P.G.: Propagation of planetary-scale disturbances from the lower into the upper atmosphere. J. Geophys. Res. (1896-1977) **66**(1), 83–109 (1961). https://doi.org/10.1029/JZ066i001p00083

Chen, X., Luo, D., Wu, Y., Dunn-Sigouin, E., Lu, J.: Nonlinear response of atmospheric blocking to early winter Barents–Kara seas warming: an idealized model study. J. Clim. **34**(6), 2367–2383 (2021). https://doi.org/10.1175/JCLI-D-19-0720.1

Domeisen, D.I.V., Butler, A.H., Charlton-Perez, A.J., Ayarzagüena, B., Baldwin, M.P., Dunn-Sigouin, E., Furtado, J.C., Garfinkel, C.I., Hitchcock, P., Karpechko, A.Y., Kim, H., Knight, J., Lang, A.L., Lim, E.P., Marshall, A., Roff, G., Schwartz, C., Simpson, I.R., Son, S.W., Taguchi, M.: The role of the stratosphere in subseasonal to seasonal prediction: 2. predictability arising from stratosphere-troposphere coupling. J. Geophys. Res. Atmos. **125**(2), e2019JD030,923 (2020). https://doi.org/10.1029/2019JD030923

Efron, B., Tibshirani, R.J.: An Introduction to the Bootstrap. No. 57 in Monographs on Statistics and Applied Probability. Chapman & Hall/CRC, Boca Raton (1993)

Elsner, J., Kossin, J., Jagger, T.: The increasing intensity of the strongest tropical cyclones. Nature **455**, 92–95 (2008). https://doi.org/10.1038/nature07234

Finke, K., Hannachi, A.: Tropospheric response to stratospheric variability via lagged quantile regression. Geophys. Res. Lett. **49**(15), e2022GL099,231 (2022). https://doi.org/10.1029/2022GL099231

Francis, J.A., Vavrus, S.J.: Evidence linking Arctic amplification to extreme weather in mid-latitudes. Geophys. Res. Lett. **39**(6), 1–6 (2012). https://doi.org/10.1029/2012GL051000

Hall, R.J., Mitchell, D.M., Seviour, W.J.M., Wright, C.J.: Tracking the stratosphere-to-surface impact of sudden stratospheric warmings. J. Geophys. Res. Atmos **126**(3), e2020JD033,881 (2021). https://doi.org/10.1029/2020JD033881

Hersbach, H., Bell, B., Berrisford, P., Hirahara, S., Horányi, A., Muñoz-Sabater, J., Nicolas, J., Peubey, C., Radu, R., Schepers, D., Simmons, A., Soci, C., Abdalla, S., Abellan, X., Balsamo, G., Bechtold, P., Biavati, G., Bidlot, J., Bonavita, M., De Chiara, G., Dahlgren, P., Dee, D., Diamantakis, M., Dragani, R., Flemming, J., Forbes, R., Fuentes, M., Geer, A., Haimberger, L., Healy, S., Hogan, R.J., Hólm, E., Janisková, M., Keeley, S., Laloyaux, P., Lopez, P., Lupu, C., Radnoti, G., de Rosnay, P., Rozum, I., Vamborg, F., Villaume, S., Thépaut, J.N.: The ERA5 global reanalysis. Q. J. Roy. Meteorol. Soc. **146**(730), 1999–2049 (2020). https://doi.org/10.1002/qj.3803

Hitchcock, P., Simpson, I.R.: The downward influence of stratospheric sudden warmings. J. Atmos. Sci. **71**(10), 3856–3876 (2014). https://doi.org/10.1175/JAS-D-14-0012.1

Honda, M., Inoue, J., Yamane, S.: Influence of low Arctic sea-ice minima on anomalously cold Eurasian winters. Geophys. Res. Lett. **36**(8), L08,707 (2009). https://doi.org/10.1029/2008GL037079

Inoue, J., Hori, M.E., Takaya, K.: The role of Barents Sea ice in the wintertime cyclone track and emergence of a warm-Arctic cold-Siberian anomaly. J. Clim. **25**(7), 2561–2568 (2012). https://doi.org/10.1175/JCLI-D-11-00449.1

Kim, K.Y., Son, S.W.: Physical characteristics of Eurasian winter temperature variability. Environ. Res. Lett. **11**(4), 044,009 (2016). https://doi.org/10.1088/1748-9326/11/4/044009

King, A.D., Butler, A.H., Jucker, M., Earl, N.O., Rudeva, I.: Observed relationships between sudden stratospheric warmings and european climate extremes. J. Geophys. Res. Atmos. **124**(24), 13,943–13,961 (2019). https://doi.org/10.1029/2019JD030480

Kodera, K., Mukougawa, H., Itoh, S.: Tropospheric impact of reflected planetary waves from the stratosphere. Geophys. Res. Lett. **35**(16), L16,806 (2008). https://doi.org/10.1029/2008GL034575

Kodera, K., Mukougawa, H., Fujii, A.: Influence of the vertical and zonal propagation of stratospheric planetary waves on tropospheric blockings. J. Geophys. Res. Atmos. **118**(15), 8333–8345 (2013). https://doi.org/10.1002/jgrd.50650

Kodera, K., Mukougawa, H., Maury, P., Ueda, M., Claud, C.: Absorbing and reflecting sudden stratospheric warming events and their relationship with tropospheric circulation. J. Geophys. Res. Atmos. **121**(1), 80–94 (2016). https://doi.org/10.1002/2015JD023359

Koenker, R., Hallock, K.F.: Quantile regression. J. Econ. Perspect. **15**(4), 143–156 (2001). https://doi.org/10.1257/jep.15.4.143

Kretschmer, M., Coumou, D., Agel, L., Barlow, M., Tziperman, E., Cohen, J.: More-persistent weak stratospheric polar vortex states linked to cold extremes. Bull. Am. Meteorol. Soc. **99**(1), 49–60 (2018a). https://doi.org/10.1175/BAMS-D-16-0259.1

Kretschmer, M., Cohen, J., Matthias, V., Runge, J., Coumou, D.: The different stratospheric influence on cold-extremes in Eurasia and North America. NPJ Clim. Atmos. Sci. **1**(44), 1–10 (2018b). https://doi.org/10.1038/s41612-018-0054-4

Luo, D., Xiao, Y., Diao, Y., Dai, A., Franzke, C.L.E., Simmonds, I.: Impact of ural blocking on winter warm Arctic–cold Eurasian anomalies. Part II: the link to the North Atlantic oscillation. J. Clim. **29**(11), 3949–3971 (2016). https://doi.org/10.1175/JCLI-D-15-0612.1

Matsuno, T.: A dynamical model of the stratospheric sudden warming. J. Atmosp. Sci. **28**(8), 1479–1494 (1971). https://doi.org/10.1175/1520-0469(1971)028<1479:ADMOTS>2.0.CO;2

Maycock, A.C., Hitchcock, P.: Do split and displacement sudden stratospheric warmings have different annular mode signatures? Geophys. Res. Lett. **42**(24), 10,943–10,951 (2015). https://doi.org/10.1002/2015GL066754

McIntyre, M., Palmer, T.: Breaking planetary waves in the stratosphere. Nature **305**, 593–600 (1983). https://doi.org/10.1038/305593a0

Mitchell, D.M., Gray, L.J., Anstey, J., Baldwin, M.P., Charlton-Perez, A.J.: The influence of stratospheric vortex displacements and splits on surface climate. J. Clim. **26**(8), 2668–2682 (2013). https://doi.org/10.1175/JCLI-D-12-00030.1

Mori, M., Watanabe, M., Shiogama, H., Inoue, J., Kimoto, M.: Robust Arctic sea-ice influence on the frequent Eurasian cold winters in past decades. Nat. Geosci. **7**, 869–873 (2014). https://doi.org/10.1038/ngeo2277

Murto, S., Caballero, R., Svensson, G., Papritz, L.: Interaction between Atlantic cyclones and Eurasian atmospheric blocking drives wintertime warm extremes in the high Arctic. Weather Clim. Dyn. **3**(1), 21–44 (2022). https://doi.org/10.5194/wcd-3-21-2022

Nath, D., Chen, W., Wang, L., Ma, Y.: Planetary wave reflection and its impact on tropospheric cold weather over Asia during January 2008. Adv. Atmos. Sci. **31**, 851–862 (2014). https://doi.org/10.1007/s00376-013-3195-8

O'Neill, A., Charlton-Perez, A., Polvani, L.: Middle atmosphere - stratospheric sudden warmings. In: North, G.R., Pyle, J., Zhang, F. (eds.) Encyclopedia of atmospheric sciences. 2nd edn., pp. 30–40. Academic Press, Oxford (2015). https://doi.org/10.1016/B978-0-12-382225-3.00230-9

Outten, S.D., Esau, I.: A link between Arctic sea ice and recent cooling trends over Eurasia. Clim. Chang. **110**(3-4), 1069–1075 (2012). https://doi.org/10.1007/s10584-011-0334-z

Panagiotopoulos, F., Shahgedanova, M., Hannachi, A., Stephenson, D.B.: Observed trends and teleconnections of the Siberian high: a recently declining center of action. J. Clim. **18**(9), 1411–1422 (2005). https://doi.org/10.1175/JCLI3352.1

Perlwitz, J., Graf, H.F.: Troposphere-stratosphere dynamic coupling under strong and weak polar vortex conditions. Geophys. Res. Lett. **28**(2), 271–274 (2001). https://doi.org/10.1029/2000GL012405

Perlwitz, J., Harnik, N.: Observational evidence of a stratospheric influence on the troposphere by planetary wave reflection. J. Clim. **16**(18), 3011–3026 (2003). https://doi.org/10.1175/1520-0442(2003)016<3011:OEOASI>2.0.CO;2>

Perlwitz, J., Harnik, N.: Downward coupling between the stratosphere and troposphere: the relative roles of wave and zonal mean processes. J. Clim. **17**(24), 4902–4909 (2004). https://doi.org/10.1175/JCLI-3247.1

Plumb, R.A.: On the three-dimensional propagation of stationary waves. J. Atmos. Sci. **42**(3), 217–229 (1985). https://doi.org/10.1175/1520-0469(1985)042<0217:OTTDPO>2.0.CO;2

Scaife, A.A., Knight, J.R., Vallis, G.K., Folland, C.K.: A stratospheric influence on the winter NAO and North Atlantic surface climate. Geophys. Res. Lett. **32**(18). https://doi.org/10.1029/2005GL023226 (2005)

Statnaia, I., Karpechko, A., Kämäräinen, M., Järvinen, H.: Stratosphere–troposphere coupling enhances subseasonal predictability of Northern Eurasian cold spells. Q. J. Roy. Meteorol. Soc., 1–15. https://doi.org/10.1002/qj.4335 (2022)

Thompson, D.W.J., Wallace, J.M.: Regional climate impacts of the Northern Hemisphere annular mode. Science **293**(5527), 85–89 (2001). https://doi.org/10.1126/science.1058958

Thompson, D.W.J., Baldwin, M.P., Wallace, J.M.: Stratospheric connection to Northern Hemisphere wintertime weather: implications for prediction. J. Clim. **15**(12), 1421–1428 (2002). https://doi.org/10.1175/1520-0442(2002)015<1421:SCTNHW>2.0.CO;2

Waugh, D.W., Polvani, L.M.: Stratospheric polar vortices. Am. Geophys. Union (AGU), 43–57. https://doi.org/10.1002/9781118666630.ch3 (2010)

Waugh, D.W., Sobel, A.H., Polvani, L.M.: What is the polar vortex and how does it influence weather? Bull. Am. Meteorol. Soc. **98**(1), 37–44 (2017). https://doi.org/10.1175/BAMS-D-15-00212.1

Wu, B., Su, J., Zhang, R.: Effects of autumn-winter Arctic sea ice on winter Siberian High. Chin. Sci. Bull. **56**(30), 3220–3228 (2011). https://doi.org/10.1007/s11434-011-4696-4

Yao, Y., Luo, D., Dai, A., Simmonds, I.: Increased quasi stationarity and persistence of winter ural blocking and Eurasian extreme cold events in response to arctic warming. Part I: Insights from observational analyses. J. Clim. **30**(10), 3549–3568 (2017). https://doi.org/10.1175/JCLI-D-16-0261.1